Impedance-based modeling of electrochemical energy storage devices – A successful implementation for NiMH batteries used in design tools for hybrid electric vehicles

Marc Thele, Maja Radin-Macukat, Dirk Uwe Sauer, Oliver Bohlen, Dirk Linzen
Institute for Power Electronics and Electrical Drives ISEA,
RWTH Aachen University, Jaegerstr. 17/19, 52066 Aachen, Germany,
Phone +49 241 80 969 45, Fax +49 241 80 922 03, E-mail batteries@isea.rwth-aachen.de

Eckhard Karden
Ford Research Center Aachen,
Suesterfeldstrasse 200, 52079 Aachen, Germany

Abstract

To handle the complexity of modern automotive power nets, simulation-based design methods are important and suitable models of all system components including the battery as a main part are therefore mandatory. However, simulation models of energy storage devices are difficult to obtain. In particular, batteries are time-variant and strongly non-linear. The paper presents an impedance-based modeling approach that copes with these characteristics and offers the development and parameterization of powerful models covering a wide dynamic range. The modeling approach has been applied to several different battery technologies. These models are already successfully used by an automotive manufacturer which reflects the applicability of this modeling approach.

As an interesting example, this paper outlines the development of a NiMH battery model. Besides the impedance-based part of the model, the influences of the typical hysteresis effect of NiMH batteries is described in detail and an appropriate modeling approach is introduced.

Key words: NiMH battery, Li-Ion battery, lead-acid battery, supercapacitor, battery model

1. Introduction

As a successful example for impedance-based modeling and as an interesting application for hybrid electric vehicles, this paper introduces the latest development of an NiMH battery model. The impedance-based core of the model (see section 2) is extended by a model part which considers the typical hysteresis phenomenon of NiMH batteries (section 3). This part of the model is parameterized in the time domain and increases the validity range of the model significantly. This shows the synergies which are available when combining the impedance-based modeling approach and models developed and implemented in the time domain.

The impedance-based modeling approach employs electrochemical impedance spectroscopy (EIS) [6]. The measurements were carried out with the *EIS*meter, an impedance spectroscope that operates in galvanostatic mode and has been developed especially for batteries and fuel cells at our institute [7]. Small-signal excitations (I_{ac}) and the evaluation of the system´s response enables accurate investigations at nearly any working point (state of charge, temperature, dc-current). The models are build by joining universal electrical components such as inductors, capacitors and (non-linear) resistors. Physico-chemical processes can easily and effectively be modeled this way providing also a minimized computation effort. The method is applicable for all kinds of electrochemical energy storage devices [1, 8].

A similar modeling approach is given in [2] for a NiMH battery, however, without considering non-linear resistances and without modeling the typical hysteresis phenomenon which significantly influences the NiMH open-circuit voltage (OCV). Unlike other battery technologies, the OCV of NiMH batteries is not unambiguously determined by the state of charge (SOC) due to this

phenomenon [3, 4]. Consequently, a detailed hysteresis model has been developed for the prediction of the OCV and is combined with the impedance-based model which determines the dynamic overvoltages during current flows.

The complete model implementation and a general overview on how to parameterize the models are given in this paper. The modeling approach is evaluated by comparing the measured and the simulated battery voltage corresponding to several current profiles with different dynamics and current rates. All investigations have been performed on cylindrical battery samples produced by Sanyo ("Hr-DP") and Panasonic ("HHR 650 D"), both rated with a nominal capacity C_N of 6.5 Ah.

2. The Impedance-Based Core of the Battery Model

Typical impedance spectra of a NiMH battery (Figure 1) show an inductive behavior (L) at high frequencies which is caused mainly by the metallic connectors of the battery. The battery shows pure ohmic resistance (R_i) at about 90 Hz . R_i reflects the limited conductance of the contacts, the active masses and the electrolyte. The semicircle is caused by charge transfer processes and charged double layers inside the battery. The changing diameter indicates the non-linearity of the charge transfer processes (resistance). To investigate this behavior, different direct current rates I_{dc} have been superimposed to the small signal excitations I_{ac}. More detailed information on this measurement procedure can be found in [1, 8].

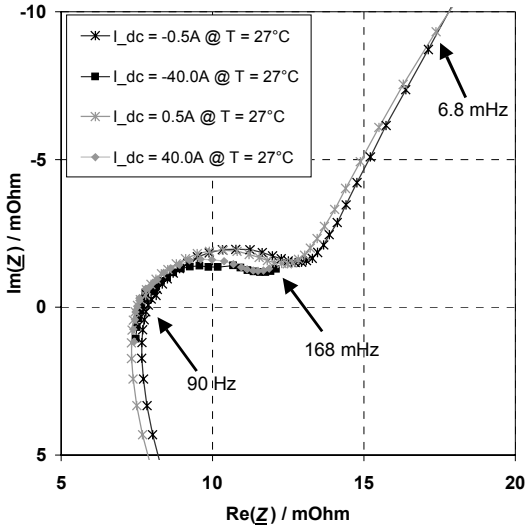

Figure 1: Impedance spectra with different superimposed direct currents I_{dc} of a NiMH battery at 70 % SOC and room temperature (battery type: Sanyo Hr-DP, 6.5 Ah)

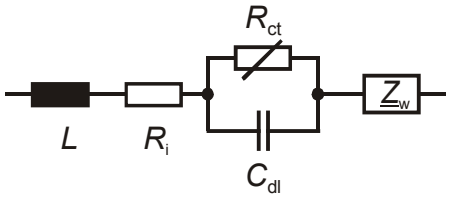

Figure 2: Equivalent electrical circuit diagram of a NiMH battery representing the overpotential during charging and discharging without modeling of the OCV

The semicircle can be modeled by a parallel connection of a non-linear resistor R_{ct} and a capacitor C_{dl}. At lower measurement frequencies (f > 168 mHz), the diffusion behavior of the battery becomes apparent which is commonly modeled by a so called Warburg impedance $\underline{Z}_w$. Based on this data, an equivalent electrical circuit of a NiMH battery can be developed and, additionally, be parameterized (Figure 1).

Particular attention has to be paid to the non-linear behavior of the charge transfer resistance R_{ct} of batteries. Generally, this behavior can be described by the so called Butler-Volmer equation with I_0 as the exchange current, n as the number of transferred elementary charges, η as the overpotential, α as a symmetry coefficient, T as the absolute temperature and k as the Boltzmann constant ($8.617 \cdot 10^{-5}$ eV/K) :

$$I = I_0 \cdot \left(\exp\left(\frac{n \cdot \alpha \cdot \eta}{k \cdot T} \right) - \exp\left(\frac{-n \cdot (1-\alpha) \cdot \eta}{k \cdot T} \right) \right) \qquad \text{Equation 1}$$

A charge transfer characteristic can also be observed for NiMH batteries. Figure 3 exemplarily illustrates the current dependent values for R_{ct} (with $R_{ct} = \frac{d\eta}{dI}$) at room temperature and 70 % state of charge (SOC). Therefore, several impedance spectra (similar to those shown in Figure 1) have been evaluated with different superimposed direct currents I_{dc} in a range from -80 A up to +80 A (~ ± 12*C* rate). The temperature and the SOC have been kept fixed as accurately as possible during the measurement because the impedance is also a function of the state of charge. To assure comparable conditions at the beginning and at the end of the measurement of one impedance spectrum, the maximum change of the state of charge during this time is limited to ΔSOC < 5%. The evaluation of R_{ct} has been carried out subsequently for each impedance measurement at different dc-current by using the equivalent circuit (Figure 2) and a least square fit routine. The points correspond to the values that arise from this fitting procedure. A Butler-Volmer behavior is observable (black solid curve), however, a constant and current independent deviation has to be solved by adding an linear resistance. A microscopic physico-chemical explanation for the offset is unknown up to date and will be subject of further research efforts. However, the final result (grey curve) is absolutely satisfying.

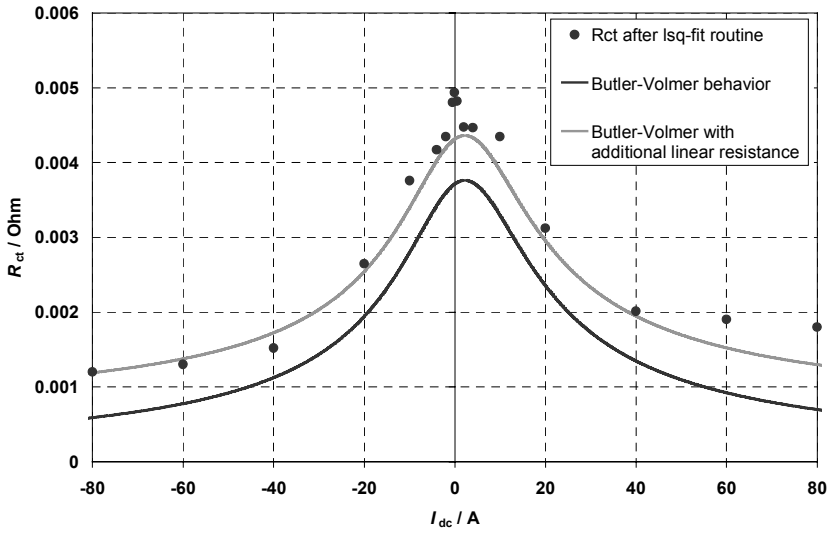

Figure 3: Non-linear Butler-Volmer behavior (charge transfer resistance) of a NiMH battery at room temperature and 70 % SOC (battery type: Sanyo Hr-DP, 6.5 Ah); black points: R_{ct} values determined by a least square fit routine, black curve: Pure Butler-Volmer behavior (n = 1, $\alpha = 0.46$, I_0 = 7 A), grey curve: Butler-Volmer behavior with an additional linear resistance of 0.6 mOhm

The resistor R_{ct} can finally be modeled by means of a series connection of a non-linear resistor R_{BV} (representing equation 1) and a linear resistor R_{add} as presented in Figure 4.

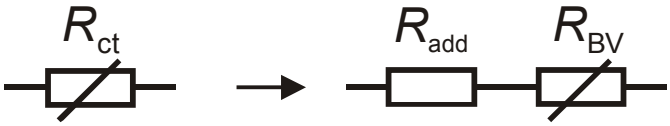

Figure 4: Detailed representation of the non-linear resistor Rct (cp. Figure 2)

The remaining components of the electrical circuit (Figure 2) have been parameterized again by using a least square fit routine. To enlarge the validity range to other temperatures and SOCs, the impedance spectra (with different I_{dc}) must be measured at various temperatures (-30°C, -18°C, -10°C, 0°C, 20°C, 40°C and 60°C) and SOCs (20, 40, 70 and 90 %). Thus, a comprehensive array of parameters can be deduced from the impedance measurements.

3. Hysteresis Phenomenon in NiMH Batteries

Generally, the OCV of a battery cell is well defined by the SOC. However, the NiMH OCV is significantly dominated by a hysteresis phenomenon unlike other battery technologies. The OCV of the NiMH battery is thus not clearly determined by SOC [3,4].

This results in a lower and an upper boundary OCV curve that can be found from measurements during constant current charging or discharging (Figure 11, schematic presentation Figure 5). Moreover, the intermediate range can be reached if the battery is operated by using shallow cycles (depicted with small cycles). If the battery is for example continuously discharged until "A" and then re-charged, the OCV (measured without current flow) will follow the upper part of the small cycle ("A" to "B") and then finally describe the outer curve until 100 % SOC. The necessity of an accurate modeling of this effect becomes obvious in Figure 6 which illustrates that the hysteresis effect can be even more significant than the dynamic overvoltages until $I_{batt} \leq 20\,\mathrm{A}$.

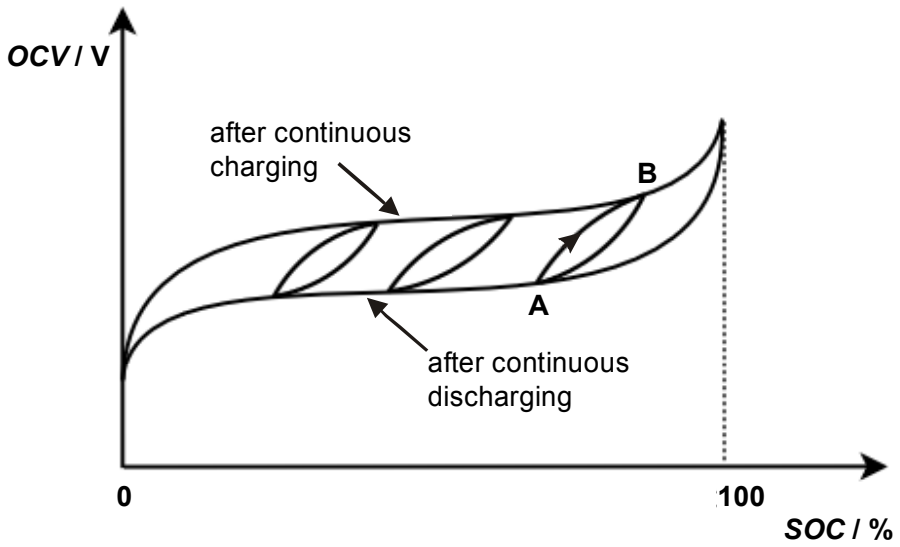

Figure 5: Schematically presentation of the hysteresis phenomenon of NiMH batteries; OCV is not clearly determined by SOC but rather dependent on pre-treatment of the battery; battery voltage is depicted without current flow

Systematic investigations showed, that the OCV depends exclusively on the charged or discharged amounts of ampere hours. Comprehensive tests and conclusions showed that the current rate does not influence the OCV level. A test with alternating discharging and charging pulses (different current rates but constant amounts of 3000 As) has been carried out (Figure 6). Rest periods of 1000 sec duration have been performed after each pulse to check the OCV which is clearly influenced by the

hysteresis effect. However, the gap between the straight lines (upper and lower OCV curves) is not affected by the current rate. This is in line with the finding in [3].

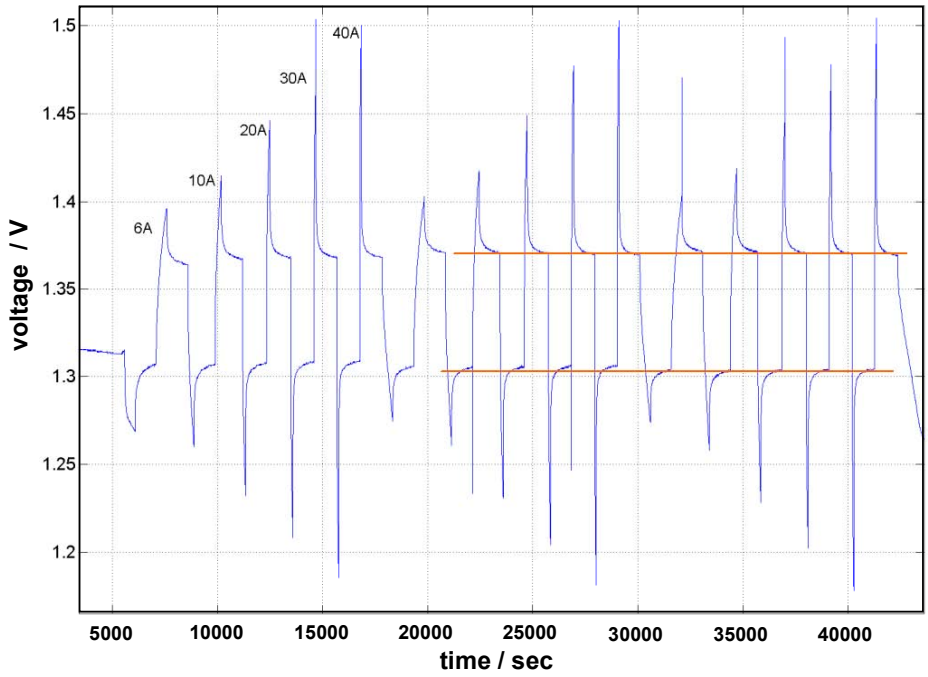

Figure 6: Alternating charging and discharging pulses with different current rates but with a constant amount of 3000 As per pulse and rest periods of 1000 sec in between; the hysteresis effect (gap between the straight lines) is independent from the current rate (battery type: Sanyo Hr-DP, 6.5 Ah / 70 % SOC, 27 °C).

3.1. Modeling of the Hysteresis Phenomenon

Generally, the OCV (U_0) of a battery cell can be modeled by a SOC-dependent voltage source. Since the NiMH OCV-behavior is seriously influenced by the above described phenomenon, the voltage source has to be adapted to a more complex model. The completed equivalent circuit is depicted in Figure 7, the detailed algorithm to calculate U_0(SOC, hyst) is discussed in the following.

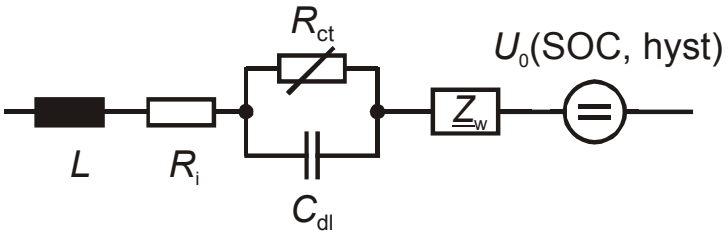

Figure 7: Equivalent electrical circuit diagram of a NiMH battery considering the OCV which shows a hysteresis effect

Basically, U_0 is calculated by the sum of the lower SOC-dependent boundary voltage U_{LB} and an additional voltage U_{hyst} which considers the hysteresis effect of partial cycling (equation 2). The maximum value of U_0 is limited by the upper boundary U_{UB}, the voltage U_{hyst} is limited SOC-dependently by the gap of the lower and upper boundary, respectively.

$$U_0(SOC) = U_{LB}(SOC) + U_{hyst} \text{ with } U_0(SOC) \le U_{UB}(SOC) \qquad \text{Equation 2}$$

Both, U_{LB}(SOC) and U_{UB} (SOC) can easily be modeled by a fixed polynomial approximation (5th order) with the SOC as the input value. The SOC is calculated according to equation 3 with I as the battery current and C_N as the nominal battery capacity (charging: $I > 0$, discharging $I < 0$). The gassing reaction can be taken into account by including the gassing current I_{gas} during the integration of the current as shown in equation 3. The gassing current is a non-linear function of temperature and potential. However, the gassing reaction has been neglected for the modeling so far ($I_{gas}=0$).

$$SOC = SOC(t=0) + \left[\frac{\int_{t=0}^{t} (I - I_{gas}) \cdot \mathrm{d}\tau}{C_N} \cdot 100 \right] \text{ with } SOC \le 100\% \qquad \text{Equation 3}$$

U_{hys} however has to be calculated during the simulation by a more complex algorithm. Therefore, a new parameter Q_{hyst} has to be defined (equation 4).

$$Q_{hyst} = \int I \cdot \mathrm{d}t \text{ with } 0 \le Q_{hyst} \le Q_{hyst\_max} \qquad \text{Equation 4}$$

Q_{hyst} sums up the charge transfer during a micro cycle of the hysteresis effect. Q_{hyst} is equivalent to 0 when the battery only has been continuously discharged and the OCV follows the lower boundary (cf. Figure 5). In case the battery is subjected to a microcycle (e.g. from "A" to "B", Figure 5), Q_{hyst} increases and is finally limited at the value Q_{hyst_max} when the upper boundary (at "B") is reached. Q_{hyst_max} has to be determined by measurements (see 3.2). U_{hyst} is consequently equal to 0 V at $Q_{hyst} = 0$ As and $U_{hyst} = U_{UB}(SOC) - U_{LB}(SOC) = U_{hyst\_max}(SOC)$ at $Q_{hyst} = Q_{hyst\_max}$. The maximum hysteresis voltage U_{hyst_max} has also to be deduced from measurements (see 3.2).

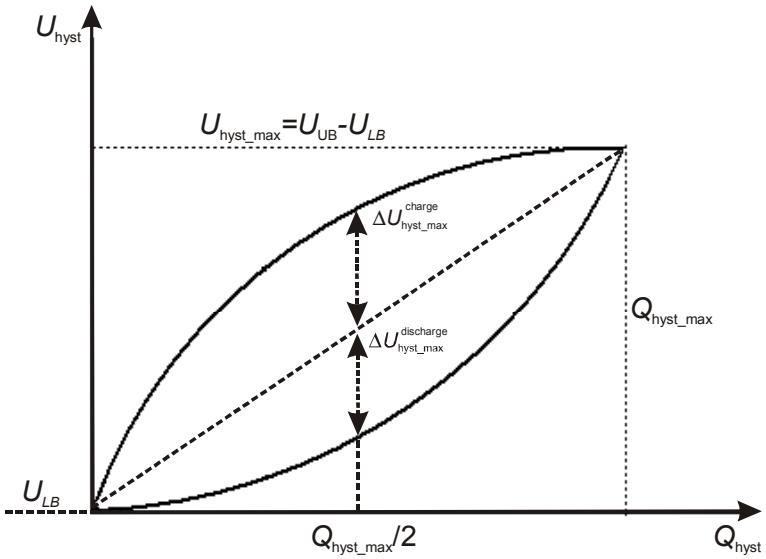

Figure 8: Closer examination of the shape of the inner course of OCV between the outer boundaries of the hysteresis curve (cp. Figure 5)

Considering these basic principles, only the shape of the course of the voltage within a microcycle between the outer boundaries has to be considered. Therefore, the maximum stretching of the inner voltage characteristic $\Delta U^{charge}_{hyst\_max}$ for charging and $\Delta U^{discharge}_{hyst\_max}$ for discharging (at $Q_{hyst\_max}/2$) have to be evaluated by measurements (see 3.2). Since the hysteresis voltage at $Q_{hyst} = 0$, at $Q_{hyst} = Q_{hyst\_max}/2$ and $Q_{hyst} = Q_{hyst\_max}$ is thus well known,

the upper curve can be approximated by a polynomial equation of second order. The same procedure is valid for the lower curve by using $\Delta U_{\text{hyst\_max}}^{\text{discharge}}$.

However, a more dynamic operation with smaller Ah throughputs than $Q_{\text{hyst\_max}}$ leads to processes inside the two depicted voltage curves. Figure 9 illustrates an appropriate test:

The battery has been continuously discharged to 70 % SOC and Q_{hyst} is set to 0 Ah. Subsequently, the battery has been charged with 10 A up to $Q_{\text{hyst}} = 0.7$ Ah (9.3 % C_N, point "B" in the graph) and $Q_{\text{hyst}} = 1.2$ Ah (18.5 % C_N, point "C") respectively. Rest periods (1000 sec) have been introduced to determine the OCV and U_{hyst} during the test. After charging to points B and to point C respectively, the battery has been discharged with -10 A until $Q_{\text{hyst}} = 0$ Ah again. A very similar symmetry of both curves ("$A \rightarrow B \rightarrow A$" and "$A \rightarrow C \rightarrow A$") can be observed considering a scaling factor which is linear to the actual amount of Q_{hyst}. This correlation can be used for modeling (equations 5 and 6).

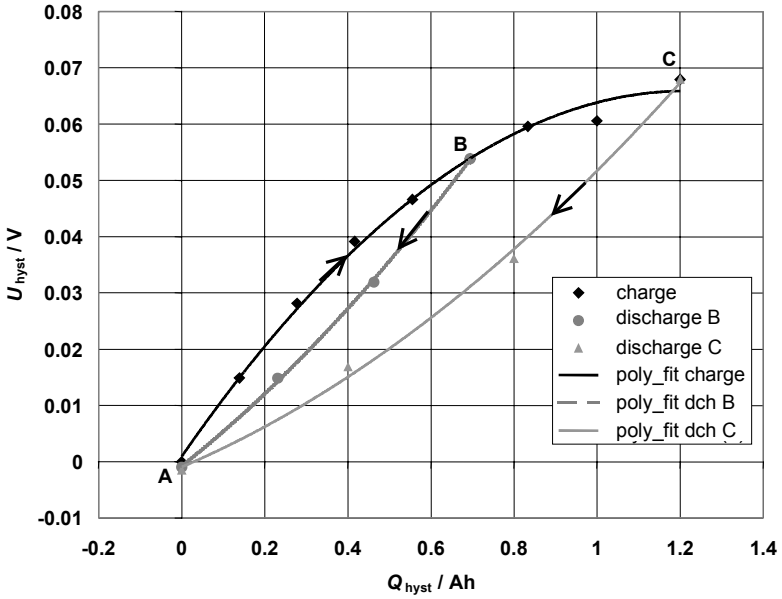

Figure 9: Measurement of the inner voltage curves between lower and upper boundary, two different discharging periods (B: after 0.7 Ah charging / C: after 1.2 Ah charging) (battery type: Sanyo Hr-DP, 6.5 Ah / 70 % SOC, 27 °C)

$$\Delta U_{\text{hyst}}^{\text{discharge}} = \Delta U_{\text{hyst\_max}}^{\text{discharge}} \cdot \frac{Q_{\text{hyst}}}{Q_{\text{hyst\_max}}} \qquad \text{Equation 5}$$

$$\Delta U_{\text{hyst}}^{\text{charge}} = \Delta U_{\text{hyst\_max}}^{\text{charge}} \cdot \frac{Q_{\text{hyst\_max}} - Q_{\text{hyst}}}{Q_{\text{hyst\_max}}} \qquad \text{Equation 6}$$

As already mentioned, the outer voltage curves (Figure 8) can be approximated by second order polynomials. Using equations 5 and 6, the same procedure can be applied when the Ah throughput is smaller than $Q_{\text{hyst\_max}}$. To explain the employed algorithm, a charging/discharging sequence is explained by means of Figure 10 as an example:

The sequence starts at point "A". Initially, the sign of the current is determined. Since the first pulse is a charging pulse, the voltage starts to rise according to the charging curve "ACB". When charging is finished at some point (here: "C"), this point corresponds to the first point of the new discharging curve "CDA". The second point is the starting point "A". The third point ("D") can be determined by considering half of the charged value (charging from "A" to

"C") and using equation 5. This is sufficient for the calculation of the polynomial coefficients for the discharging curve "CDA".

Instead of a finished discharging to point "A", the discharging may be finished in point "E" and charging starts again. The first point for the calculation of the next charging period is point "E", the second is again the saturation point B. For the calculation of the charging curves, point "B" is always relevant as the reference point, and for the calculation of the discharging curve point "A" is the reference point. The still needed third point for the coefficients of the new charging curve ("EFB") can be calculated again by using the similarity (equation 6).

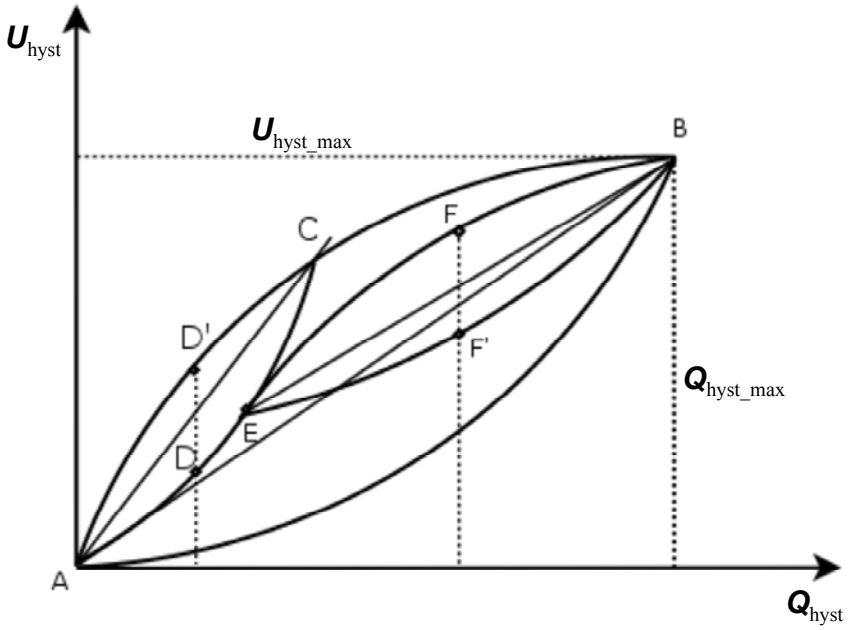

Figure 10: Exemplary illustration of the modeling of $U_{hsyt}(Q_{hyst})$ when the battery charge throughput is smaller than Q_{hyst_max}

3.2. Parameterization of the Hysteresis Phenomenon

In the following paragraphs details are given on how to parameterize the model for the hysteresis.

Determination of U_{LB}(SOC) and U_{UB}(SOC):

Measurement results to parameterize the lower and the upper boundary are illustrated in Figure 11. Therefore, a fully charged NiMH battery (nominal capacity 6.5 Ah) has been discharged with a current rate of I = -10 A and rest periods of 1000 sec after discharging of 10 % of the nominal capacity have been made for the OCV measurements. Subsequently, the battery has been fully charged (I = 10 A) using the same procedure. As already mentioned, polynomials of higher order (e.g. 5th) can be used for modeling.

Determination of Q_{hyst_max}, $\Delta U^{charge}_{hyst\_max}$ and $\Delta U^{charge}_{hyst\_max}$:

For the determination of these parameters, the already presented measurement procedure (Figure 9) has been applied at four different SOC values (5, 20, 40 and 70%). Saturation values of $Q_{hyst\_max} \approx 0.8...1.2\,\text{Ah}$ have been found. The maximum stretching of the inner voltage curves have been $\Delta U^{charge}_{hyst\_max} \approx 17...20\,\text{mV}$ and $\Delta U^{discharge}_{hyst\_max} \approx 5...10\,\text{mV}$. The stretching during charging was always significantly higher than in case of discharging. The values have

been determined for cylindrical NiMH batteries with $C_N = 6.5$ Ah (samples from Sanyo and Panasonic).

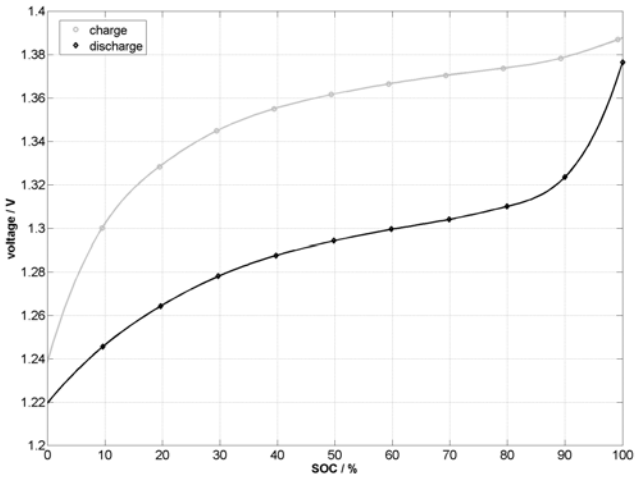

Figure 11: Measured OCV values of a NiMH battery (points); lower curve measured during discharging (-10 A) with rest periods (1000 sec) in between, upper curve during charging (+10 A); (battery type: Panasonic HHR 650 D, 6.5 Ah / 27 °C)

Determination of U_{hyst_max}:

The maximum hysteresis voltage $U_{hyst\_max}(SOC)$ corresponds to the difference of $U_{UB}(SOC)$ and $U_{LB}(SOC)$. Values of up to 70 mV have been found.

$$U_{hyst\_max}(SOC) = U_{UB}(SOC) - U_{LB}(SOC) \qquad \text{Equation 7}$$

4. Model Evaluation

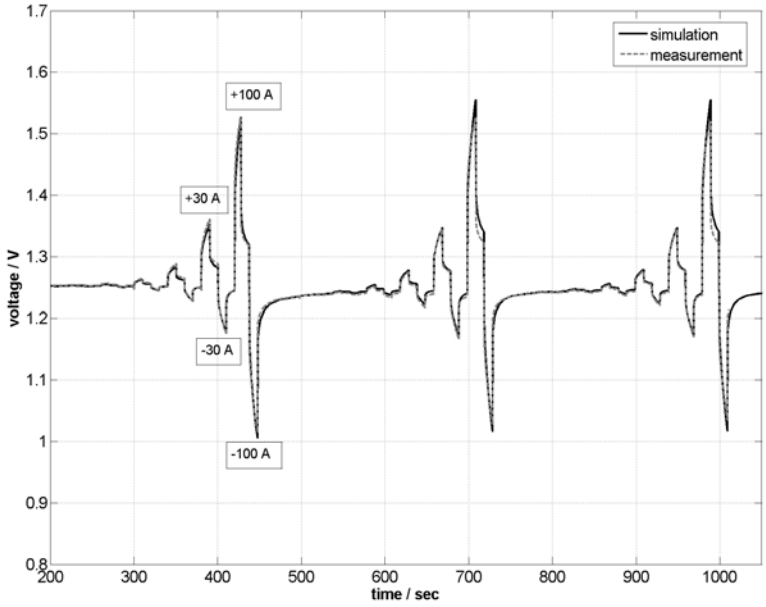

Figure 12: Comparison of measured and simulated battery voltage corresponding to an alternating profile with absolute battery currents up to 100 A at 20 % SOC and room temperature (battery type: Sanyo Hr-DP, 6.5 Ah)

Comparisons among measured and simulated voltage curves over time are presented in this section. Current profiles with different dynamics (respectively pulse duration) and a wide range of current rates have been applied to the battery.

As a first example, Figure 12 gives a comparison of the measured voltage and the voltage simulated with the model presented above for input currents in a range from 0.5 to 15 times the *C*-rate at room temperature and 20 % SOC. Alternating current pulses with 10 seconds duration followed by 10 seconds rest periods have been carried out.

Figure 13 depicts a comparison for input currents in a range from 0.5 to 4.6 times the *C*-rate at room temperature and 70 % SOC. Alternating current pulses with a lower dynamic of 100 seconds duration followed by 100 seconds rest periods have been performed.

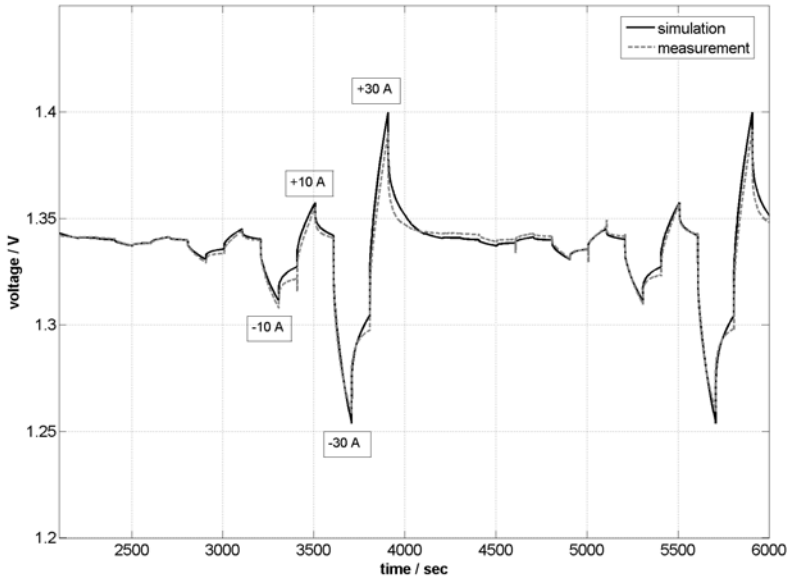

Figure 13: Comparison of measured and simulated battery voltage corresponding to an alternating profile with absolute battery currents up to 30 A at 70 % SOC and room temperature (battery type: Sanyo Hr-DP, 6.5 Ah)

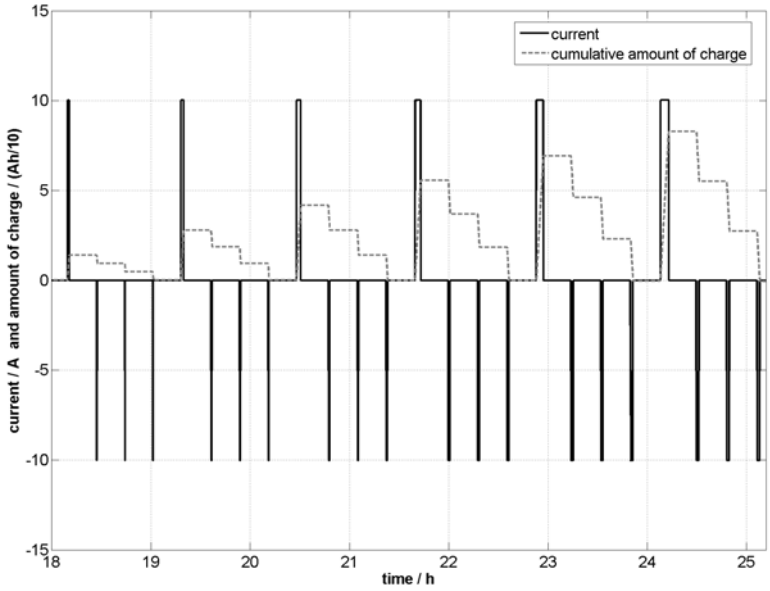

Figure 14: Input current profile to force the hysteresis effect, the discharged amount of each discharge triple corresponds to the preceding charging step

Furthermore, a special current profile that forces the hysteresis effect has been applied which illustrates the advantages of the actual hysteresis model. Therefore, current pulses with 10 A have been applied, however with different duration and therefore different amounts of charge.

The current profile is given in (Figure 14) The cumulative amount of charge of the three consecutively repeated discharge pulses corresponds to the amount of Ah of the preceding charging step. Moreover, the total amount of charged Ah has been increased subsequently. Hence, hysteresis curves of different sizes (cp. Figure 9) have to be simulated accurately to match the measured voltage (Figure 15).

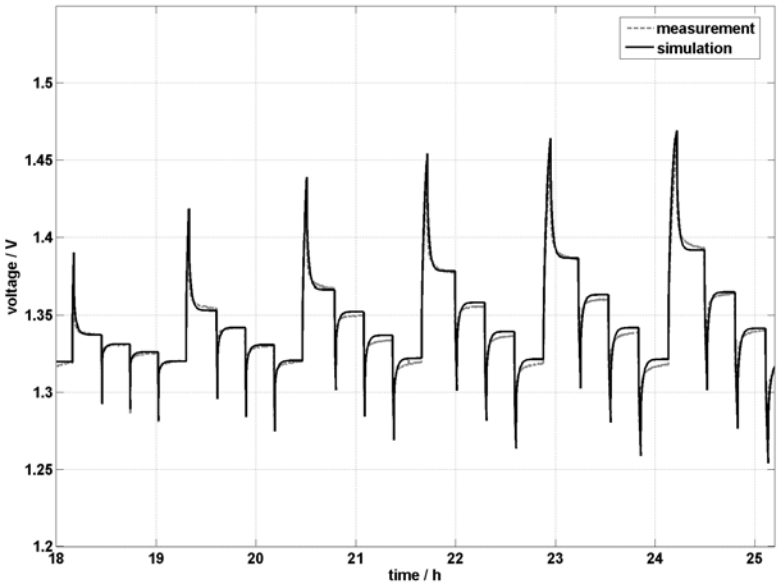

Figure 15: Voltage response to the current profile which is depicted in Figure 14 at room temperature and 70 % SOC (battery type: Sanyo Hr-DP, 6.5 Ah)

5. Discussion

An accurate consistence between the simulated and the measured battery behavior has been demonstrated in section 4. These results have been achieved by combining the impedance-based model core which describes the battery dynamic in a wide range and a hysteresis model that successfully describes the hysteresis of the open-circuit voltage in NiMH batteries. However, the hysteresis model is a phenomenological approach and has only been investigated for the two battery types produced by Sanyo ("HR-DP") and Panasonic ("HHR-650-D"). More theoretical explanation for the hysteresis phenomenon (valid for all NiMH batteries) would be beneficial for the understanding and model parameterization. The hysteresis phenomenon of NiMH batteries has been previously investigated (e.g. in [3] and [5]) and explained on a qualitative basis, but no consistent model that explains the effect quantitatively has been presented.

Within this paper measured data have been shown for room temperature only. However, the impedance based modeling approach has shown its validity and robustness also for other battery temperatures in the range of -30 °C to 50 °C. For the hysteresis of the open-circuit voltage measurements and parameter identifications for the model have been done in the full temperature range.

Since the gassing reaction is an important part of the electrochemical reactions inside NiMH batteries, the battery model should be extended by an appropriate gassing model. A gassing branch with a non-linear resistor connected in parallel to the RC-element, the Warburg impedance and the OCV calculation (Figure 7) has been proven for lead-acid battery to work perfectly. [9].

Further effects that presumably have to be modeled are overcharging effects. Generally, depletion effects occur when quite high charging current rates are applied to a battery or when a battery is charged at high levels of SOC. Those effects lead to a limited charge acceptance of the battery and can compromise consequently intended operation modes of systems in which the battery is employed (e.g. recuperative braking in hybrid or electric vehicles). For lead-acid batteries such an overcharging model has been developed and implemented successfully [9]. However, for the NiMH battery the electrochemical processes need to be evaluated carefully before implementing the appropriate model.

6. Summary

An impedance-based modeling approach, that copes with the specific battery characteristics and offers the development and parameterization of powerful models covering a wide dynamic range, has been presented using the NiMH battery (section 2) as an example. This modeling approach has been successfully applied to further battery technologies such as Li-ion, lead-acid, and electrochemical double-layer capacitors [8].

Besides the impedance-based part of the model, the typical hysteresis in the open circuit voltage, which is very pronounced for NiMH batteries has been described in detail and an appropriate modeling approach has been introduced (section 3). Finally, the NiMH battery model has been convincingly evaluated with comparisons among measured and simulated voltage responses data in the time domain by using input current profiles at different states of charge, with significantly different current rates and various time constants (section 4).

The limits and valuable upgrades of the NiMH battery model have been finally discussed in section 5. Mainly, a gassing model and an overcharging model that simulates the charge acceptance of the battery need to be employed.

References

[1] S. Buller, M. Thele, E. Karden, R. De Doncker: Impedance-based non-linear dynamic battery modeling for automotive applications, J. Power Sources 113 (2003) 422-430

[2] E. Kuhn, C. Forgez, P. Lagonotte, G. Friedrich: Modeling NiMH battery using Cauer and Foster structures, J. Power Sources (Article in press, accepted 2005, available online)

[3] M. Verbrugge, E. Tate: Adaptive state of charge algorithm for nickel metal hydride batteries including hysteresis phenomena, J. Power Sources 126 (2004) 236-249

[4] K. Bundy, M. Karlsson, G. Lindbergh, A. Lundqvist: An electrochemical impedance spectroscopy method for prediction of the state of charge of a nickel-metal hydride battery at open circuit and during discharge, J. Power Sources 72 (1998) 118-125

[5] V. Srinivasan, J.W. Weidner, J. Newman: Hysteresis during Cycling of Nickel Hydroxide Active Material, J. Power Sources 148 (2001) 969-980

[6] J.R. Macdonald, Editor, Impedance Spectroscopy, Emphasizing Solid Materials and Systems, John Wiley & Sons (1987) ISBN: 0-471-83122-0

[7] H. Blanke, T. Sanders, M. Kiel, T. Baumhöfer, B. Fricke, D.U. Sauer: EISmeter – The art of impedance spectroscopy on batteries and fuel cells, Technische Mitteilungen 99 (2006) No 1&2, p. 231-234, ISSN: 0040-1439

[8] S. Buller: Impedance-based simulation models for energy storage devices in advanced automotive power systems, PhD thesis, RWTH Aachen University, 2002, ISBN: 3-8322-1225-6

[9] M. Thele, E. Karden, E. Surewaard, D.U. Sauer: Impedance-based overcharging and gassing model for VRLA/AGM batteries, J. Power Sources (Article in press, accepted 2005, available online)

Authors

Marc Thele, Dipl.-Ing., ISEA, RWTH Aachen University, Germany

Phone: +49 241 80 96945, Fax: +49 241 80 92203, te@isea.rwth-aachen.de

M. Thele accomplished his diploma thesis at the Institute for Electrical Drives and Power Electronics (ISEA) and received his Diploma in Electrical Engineering in 2002 from RWTH University Aachen, Germany. In June 2002, he joined the ISEA as a research associate. His research activities are in the area of modeling and simulation of different battery technologies.

Dirk Uwe Sauer, Prof. Dr. rer. nat., ISEA, RWTH Aachen University, Germany
Phone: +49 241 8096977, Fax: +49 241 8092203, sr@isea.rwth-aachen.de

D. U. Sauer received his diploma in Physics in 1994 from University of Darmstadt. From 1992-2003 he has been research scientist and senior scientist at Fraunhofer Institute for Solar Energy Systems ISE in Freiburg/Germany. In 2003 he received his PhD at Ulm University on battery modeling and system optimization. Since 10/2003 he is Juniorprofessor at RWTH Aachen University for “Electrochemical Energy Conversion and Storage Systems”

Eckhard Karden, Dr.-Ing. Dipl.-Phys., FFA Ford Forschungszentrum Aachen, Süsterfeldstr. 200, D-52072 Aachen, Germany
Phone: +49-241-9421-337, e-mail: ekarden@ford.com.

E. Karden is Research Engineer for storage systems in the Energy Management group of Ford’s European Research Center in Aachen (FFA). Before he joined Ford in 2002, he was Chief Engineer of the Institute for Power Electronics and Electrical Drives (ISEA) of Aachen University of Technology (RWTH), where he had completed his Ph.D. thesis on impedance spectroscopy of batteries under Professor De Doncker.